Journal of the Korean Ceramic Society
Vol. 48, No. 6, pp. 549~558, 2011.

http://dx.doi.org/10.4191/kcers.2011.48.6.549

Application of Generalized Transmission Line Models to Mixed Ionic-Electronic Transport Phenomena

Pyung-An Ahn, Eui-Chol Shin, Gye-Rok Kim, and Jong-Sook Lee†

School of Materials Science and Engineering, Chonnam National University, Gwangju 500-757, Korea

(Received November 8, 2011; Revised November 23, 2011; Accepted November 23, 2011)

ABSTRACT

Application of a generalized equivalent circuit including the electrode condition for the Hebb-Wagner polarization in the frequency domain proposed by Jamnik and Maier can provide a consistent set of material parameters, such as the geometric capacitance, partial conductivities, chemical capacitance or diffusivity, as well as electrode characteristics. Generalization of the shunt capacitors for the chemical capacitance by the constant phase elements (CPEs) was applied to a model mixed conducting system, Ag_2S, with electron-blocking AgI electrodes and ion-blocking Pt electrodes. While little difference resulted for the electron-blocking cell with almost ideal Warburg behavior, severely non-ideal behavior in the case of Pt electrodes not only necessitates a generalized transmission line model with shunt CPEs but also requires modelling of the leakage in the cell approximately proportional to the cell conductance, which then leads to partial conductivity values consistent with the electron-blocking case. Chemical capacitance was found to be closer to the true material property in the electron-blocking cell while excessively high chemical capacitance without expected silver activity dependence resulted in the electron-blocking cell. A chemical storage effect at internal boundaries is suggested to explain the anomalies in the respective blocking configurations.

Key words : Impedance, Modelling/models, Silver/silver compounds, Electrochemistry, Electrical conductivity

1 Introduction

Mixed ionic-electronic conduction plays critical functional roles in solid state electrochemical devices such as fuel cells, batteries, electrochemical sensors, and electrochromic devices. For the electrode materials in these electrochemical devices, high ionic transport as well as electronic transport is beneficial and often necessary. The mixed conducting oxides can also be applied to gas permeation membranes.[1] For all solid state electrochemical devices,the electronic conductivity must be minimized to prevent losses from leakage currents. Mixed ionic-electronic conduction is also a critical issue in state-of-the-art electronics employing various nonmetallic ionic crystals. Ionic conduction in dielectric materials and oxide semiconductors is mostly undesirable.It is responsible for the degradationof the electronic components and devices such as multi-layer capacitors, varistors, and oxide transistors under a high operating dc field. The degradation of ceramic electronic components such as multilayer ceramic capacitors (MLCC) can also be ascribed to mixed conduction.[2]

Theoretical background and experimental demonstrations of impedance spectroscopy as a tool for chemical and electrochemical analyses of mixed conductors have been reported[3-7], which is no other than the frequency domain representation of the non-steady state Hebb-Wagner polarization/relaxation in mixed conductors using electrodes that selectively block electrons or ions[8-14] Stoichiometry polarization is induced across the specimen by the blocked charge species, and transport of the non-blocked species in the material is thus accomplished by chemical diffusion under the activity gradient (rather than by conduction driven by the electric field). The dc steady state behavior for the conduction of the unblocked minority charge carriers[8-10,12] can be measured. In addition, it is possible to monitor the time-dependence of polarization or depolarization, which provides the chemical diffusion coefficient D_{chem} from the relaxation behavior and possibly the total bulk conductivity from the IR drop.[13] The polarization behavior in the time domain can be equivalently represented in the frequency domain by a Fourier-Laplace transformation.[15-17] In contrast to the piecewise evaluation of the time-domain response, the generalized equivalent circuit shown in Fig. 1(a) describes the overall frequency response and all the material and additional cell parameters can be systematically and self-consistently obtained by a single-step analysis.[3-7]

Although the idealized equivalent circuit in Fig. 1(a) has been successfully demonstrated for Ag_2S with electron-blocking AgI | Ag electrodes[7] and Sm-doped ceria (SDC) with ion-blocking Pt electrodes,[6] general applications are expected to be quite limited, since it is rather the exception than the rule that the real systems can be described by an ideal resistor and capacitor elements. The Jamnik-Maier model and the generalization of the capacitors to the constant phase elements (CPEs) of a complex capacitance $A(iw)^{\alpha-1}$ have recently been implemented in the commercial analysis program Zview

†Corresponding author : Jong-Sook Lee
E-mail : jongsook@jnu.ac.kr
Tel : +82-62-530-1701 Fax : +82-62-530-1699

(Scribner Ass.)[18] upon request by one of the present authors (J.-S. Lee). In the present work, facilitated by such advances, the previous report on the impedance behavior of Ag_2S with AgI electrodes[7] is reassessed. Furthermore, the analysis is further extended to an ion-blocking $Pt|Ag_2S|Pt$ symmetrical cell.

2. Background

The full derivation of the analytical expression of the impedance of the circuit of Fig. 1(a) has been previously reported.[3-6] If we omit the contribution of C_{dielec} for the purpose of clarity, define the interfacial impedances, $Z^{\perp}_{ion(eon)} \equiv R^{\perp}_{ion(eon)} / (1+i\omega R^{\perp}_{ion(eon)} C^{\perp}_{ion(eon)})$, and express the product $(R_{ion}+R_{eon})C_{chem}$ by D_{chem}, the impedance can then be expressed as:

$$Z(\omega) = Z_{\infty} + (Z_0 - Z_{\infty}) \frac{\left(1+\frac{R_{ion}+R_{eon}}{2(Z^{\perp}_{ion}+Z^{\perp}_{eon})}\right)\tanh\sqrt{\frac{i\omega L^2}{4D_{chem}}}}{\sqrt{\frac{i\omega L^2}{4D_{chem}}} + \frac{R_{ion}+R_{eon}}{2(Z^{\perp}_{ion}+Z^{\perp}_{eon})}\tanh\sqrt{\frac{i\omega L^2}{4D_{chem}}}} \quad (1)$$

The high and low frequency impedances, Z_{∞} and Z_0, are defined as:

$$Z_{\infty} \equiv \frac{R_{ion}R_{eon}}{R_{ion}+R_{eon}} + 2\frac{Z^{\perp}_{ion}Z^{\perp}_{eon}}{Z^{\perp}_{ion}+Z^{\perp}_{eon}} \quad (2)$$

and

$$\frac{1}{Z_0} \equiv \frac{1}{R_{ion}+2Z^{\perp}_{ion}} + \frac{1}{R_{eon}+2Z^{\perp}_{eon}} \quad (3)$$

It is necessary to point out that the Warburg diffusion impedance is represented by an *RC* transmission line model, since the governing equations for the matter diffusion in a medium and the electrical signal propagation in the transmission line are mathematically analogous, viz. the electrical signal transmission equation

$$\frac{\partial V}{\partial t} = \frac{1}{RC}\frac{\partial^2 V}{\partial x^2} \quad (4)$$

versus Fick's 2nd law of diffusion

$$\frac{\partial c}{\partial t} = D\frac{\partial^2 c}{\partial x^2} \quad (5)$$

The impedance of the two rail transmission line model shown in Fig. 1(a) with one ideally blocking terminal condition $(R^{\perp} \to \infty)$ without interfacial charging represented by $C^{\perp}$ and the other short-circuited $(R^{\perp} \to 0)$ thus becomes a half tear-drop shape response represented by

$$Z = R_{bulk} + Z_W = R_{bulk} + (R_{dc} - R_{bulk})\frac{\tanh\sqrt{i\omega(R_{ion}+R_{eon})C_{chem}/4}}{\sqrt{i\omega(R_{ion}+R_{eon})C_{chem}/4}} \quad (6)$$

where R_{dc} is the resistance of the minority charge carriers

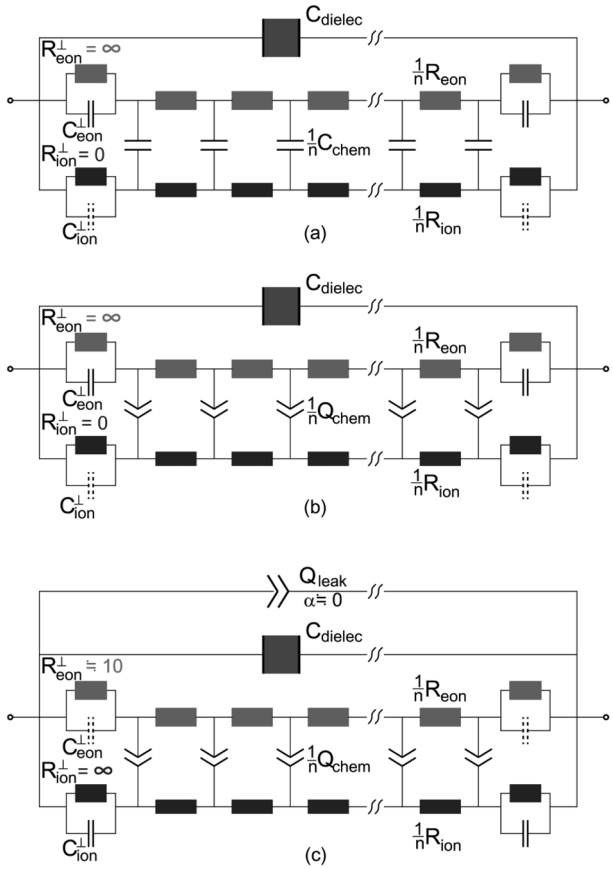

Fig. 1. Generalized equivalent circuit used for an electron-blocking symmetrical cell $Ag|AgI|Ag_2S|AgI|Ag$ that can be generally applied to a mixed conductor with thickness much greater than the Debye length λ. The quantities, R_{ion}, R_{eon}, and C_{chem}, which all refer to the overall sample, are weighted by $1/n$, with n being the number of transmission line unit cells.[3] (b) Shunt capacitors for C_{chem} replaced by CPEs or Q elements can represent the generalized Warburg behavior with the electrode effects included. (c) Strongly non-ideal behavior of the ion-blocking symmetrical cell $Pt|Ag_2S|Pt$ was successfully described by modelling a leakage across the cell Q_{leak} with $\alpha \approx 0$ and non-zero electrode resistance for electronic flow $R^{\perp}_{eon} \approx 10\Omega$.

allowed to pass through the cell (either R_{ion} or R_{eon}) and R_{bulk} corresponds to $(R^{-1}_{ion} + R^{-1}_{eon})^{-1}$.

The establishment of a stoichiometry gradient in the Hebb-Wagner polarization can be described by the transport along the transmission line by charging of the capacitors in the transverse direction. The transverse capacitors thus represent the chemical capacitance, which, in the case of dilute concentration of charge carriers, can be represented as

$$C_{chem} = \frac{q^2}{kT}SL\left(\frac{1}{z^2_{ion}c_{ion}} + \frac{1}{z^2_{eon}c_{eon}}\right)^{-1} \quad (7)$$

and related with the chemical diffusion coefficient as

$$D_{chem} = \frac{L^2}{(R_{ion}+R_{eon})C_{chem}} \quad (8)$$

where S and L represent the area and length of the sample. In contrast to the electrostatic capacitances, C_{chem} is proportional to the sample volume.

It should be also noted that the resistance and capacitance of the electrodes, $R^{\perp}_{ion(eon)}$ and $C^{\perp}_{ion(eon)}$, are of a functional origin with respect to the mixed conductor, not the property of the electrode materials. For an ideally reversible and blocking electrode, $R^{\perp}_{ion(eon)}$ is 0 and ∞, respectively. It should be noted that the interfacial impedances, $Z^{\perp}_{ion(eon)} \equiv R^{\perp}_{ion(eon)}/(1+i\omega R^{\perp}_{ion(eon)}C^{\perp}_{ion(eon)})$, become zero for ideally reversible electrodes with $R^{\perp}_{ion(eon)}=0$ but are purely capacitive for an ideally blocking electrode with infinite $R^{\perp}_{ion(eon)}$ with electrostatic double layer capacitance $C^{\perp}_{ion(eon)}$, given as follows:

$$C^{\perp}_{ion(eon)} = \varepsilon\varepsilon_{\circ}\frac{S}{\lambda_{ion(eon)}} = S\sqrt{\frac{q^2 c_{ion(eon)}}{\varepsilon\varepsilon_{\circ}kT}} \tag{9}$$

As emphasized previously,[7] the presence of the electrostatic capacitance due to the blocking condition may be considered a "key signature" that distinguishes electrochemical Hebb-Wagner polarization from purely chemically induced relaxation. Since $C^{\perp}_{ion(eon)}$, when comparable to C_{chem}, can substantially affect the Warburg impedance, caution should be taken with the use of the high frequency part of the Warburg impedance (or equivalently short-time dc relaxation) in evaluation of the diffusion parameters based on a formulation by Fick's law only. This aspect has been neglected in the earlier work.[15-17]

For the conductive systems where the resistance effects are of the main interest, the non-ideal behavior is attributed to the capacitance effects, which are thus described by so-called constant phase elements (CPEs) or Q according to Boukamp's convention.[20] The spectrum of a Q element exhibits a constant phase of $\alpha\pi/2$ in the Z' vs. $-Z''$ impedance plane

$$Z^{*}_{Q} = [A(i\omega)^{\alpha}]^{-1} = A^{-1}\omega^{-\alpha}\exp\left(-i\alpha\frac{\pi}{2}\right) \tag{10}$$

and $(1-\alpha)\pi/2$ in the complex capacitance plane C' vs. C'' of $C^{*} = (i\omega Z^{*})^{-1} = C' - iC''$,

$$C^{*}_{Q} = A(i\omega)^{\alpha-1} = A\omega^{\alpha-1}\exp\left[i(\alpha-1)\frac{\pi}{2}\right] \tag{11}$$

With CPEs generalized from the ideal capacitors with $\alpha = 1$ semicircular impedance response of RC parallel circuit becomes a depressed circle or an arc shape response of the RQ circuit.It should be noted that the element was originally introduced for the non-ideal resistor elements for the non-Debye dielectric response, where α deviates from the ideal zero value for the resistors.[19] The RC transmission line for the ideal Warburg response becomes the so-called 'generalized' Warburg response with Warburg exponent $n = \alpha/2 < 0.5$ when the shunt capacitors are replaced by CPEs with $\alpha < 1$. Neglecting the interfacial capacitance for clarity, the impedance response can be written as

$$Z_{GW} = (R_{dc} - R_{bulk})\frac{\tanh\sqrt{(i\omega)^{\alpha}(R_{ion}+R_{eon})A/4}}{\sqrt{(i\omega)^{\alpha}(R_{ion}+R_{eon})A/4}} \tag{12}$$

The effective chemical capacitance or Q_{chem} and D_{chem} may be estimated from $\tau_{W\alpha}$,

$$\tau_{W\alpha} = \left(\frac{(R_{ion}+R_{eon})A}{4}\right)^{1/\alpha} = \frac{(R_{ion}+R_{eon})Q_{chem}}{4} = \frac{L^2}{4D_{chem}} \tag{13}$$

Then the generalized Warburg impedance corresponds to the fractional or anomalous diffusion processes with

$$\frac{\partial^{\alpha}c}{\partial t^{\alpha}} = D_{chem}\ \frac{\partial^2 c}{\partial x^2} \tag{14}$$

where α represents the fractional derivatives. The origin of the generalized Warburg impedance or of the CPE-like shunt capacitors in the present formalism may be thus found in the origin of the anomalous diffusion phenomena observed in many different types of materials and systems. The distribution of the relaxation times due to the inhomogeneities of various types in the real system often leads to CPE behavior as well as the generalized Warburg behavior for the limited frequency range.

For the ideal model shown in Fig. 1(a), a Fortran program originally coded by Jamnik has been applied for the ideal circuit in analysis of the experimental impedance.[7,21] Fitting was performed by the nonlinear least squares minimization but the program was not fully developed to provide the errors of the individual fit parameters, since it is not necessary for the theoretical investigation of the impedance models.[3-5,22] It was belatedly learned when the analysis of Ag_2S with AgI electrodes was ready for publication in 2009 that the 'Jamnik-Maier' model (DX-15) had been implemented in a commercial analysis program, Zview, for W. Lai and used for the analysis of Sm-doped ceria with Pt electrodes reported in 2005.[6] In the publication by Lai, however, the errors associated with fit parameters were still not provided.

The Jamnik-Maier model in the Zview program recently has been further expanded by Derek Johnson upon request by one of the authors of the present work (J.-S. Lee) as the Jamnik-Maier-Lai-Lee model (DX-19), in which all the capacitor elements in the equivalent circuit can be now generalized to CPEs.[18] Although the generalized Warburg impedance model in the functional form represented by Eq. 12 with three fit parameters, i.e. $Z_{GW} = R_{GW}\tanh(i\omega\tau_{GW})^{\alpha/2}/(i\omega\tau_{GW})^{\alpha/2}$, has been available, the modelling for the full circuit, as shown in Fig. 1, including the electrode impedance, as represented in Eq. 1 for the ideal case, has not been previously reported. Using the circuit elements of R, C or Q as input fit parameters, is also often more advantageous for obtaining direct and concrete information than the often employed parameters such as the relaxation times τ and prefactors. The generalized transmission model, DX-19, recently has been successfully applied for the analysis of a percolating carbon network in a dielectric matrix where the

fit parameters could be directly related to the transmission line parameters of R and C or Q for non-ideal behavior.[23,24] The ac response of the carbon network is not related with diffusion phenomena but from the real transmission-line like network behavior.

3. Experimentals

An electron-blocking symmetric cell Ag|AgI|Ag_2S|AgI|Ag was constructedas described elsewhere.[7] In addition, an ion-blocking symmetric cell Pt|Ag_2S|Pt was also prepared. The dimensions of the Ag_2S specimens for the electronically and ion-blocking polarization cells were $0.165 \times 0.185 \times 1.5$ cm^3 and $0.305 \times 0.085 \times 1.5$ cm^3, respectively. The impedance was measured at 160°C in the frequency range from 10^7 to ~10^{-3} Hz using a Solartron 1260 (UK, Schlumberger). A galvanic cell Pt|Ag_2S|AgI|Ag using Pt wire wound around an Ag_2S specimen controlled the silver activity (a_{Ag}) by applying the potential EMF = $-(RT/F)\ln a_{Ag}$ with respect to Ag using a constant voltage source (Keithley 228) before each impedance measurement long enough for equilibration.

4 Results and Discussion

4.1. Ag|AgI|Ag_2S|AgI|Ag electron-blocking cell

Fig. 2 shows the spectra of the cell Ag|AgI|Ag_2S|AgI|Ag

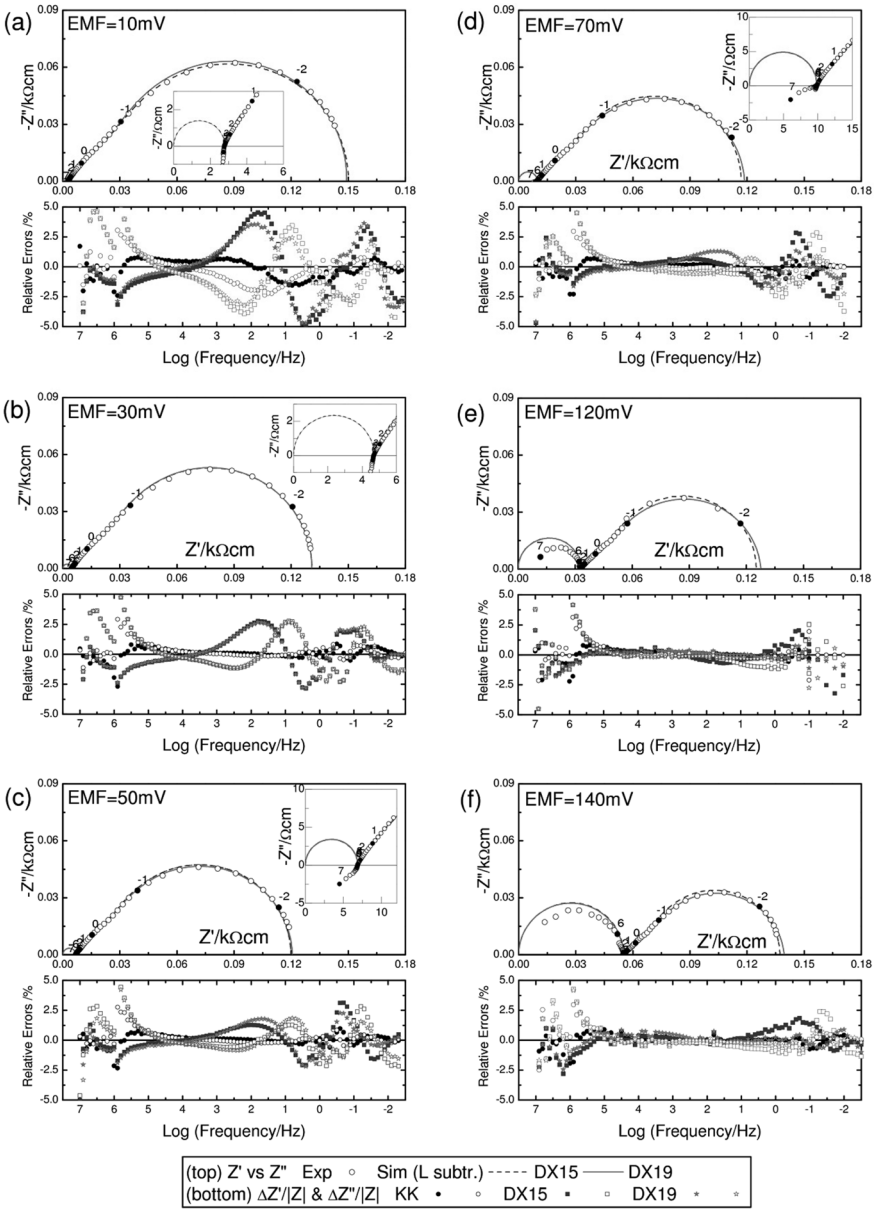

Fig. 2. Impedance spectra of Ag|AgI|Ag_2S|AgI|Ag with EMF of the galvanic cell of 10, 30, 50, 70, 120, and 140 mV. The lines indicate the simulation according to the fit results using the generalized equivalent circuit in Fig. 1 (DX15) and with chemical capacitors replaced by CPEs (DX19). In the simulated curves the inductor elements were subtracted.

for EMF = 10, 30, 50, 70, 120, and 140 mV. A half-tear shape Warburg impedance response is clearly indicated in all the spectra. A similar spectral feature has been reported for Ag_2Te using the cell configuration of Ag | AgI | Ag_2Te | AgI | Ag.[25]

In the respective bottom graphs Kramers-Kronig (KK) residuals, $(Z_{exp} - Z_{sim})/|Z^*_{sim}|$ are indicated for real and imaginary impedances, respectively. Conducting KK tests before the model analysis is recommended, since poorly fit results may be due to the poor quality of the impedance data rather than the model inadequacy. The results indicate the measured data for the low EMF (or high silver activity) exhibit substantially large KK residuals up to 2.5%. The poor data quality just below 1 MHz is ascribed to the intrinsic problem of the particular instrument used in the present study. Despite the flawed measurement, the fitting of the data including those above 1 MHz was found to provide more reliable estimation of the model parameters. On the other hand, the low frequency impedance tends to strongly increase instead of reaching the dc limit indicated by the simulated curves (not shown). The phenomena disappeared or lessened when the cell components, i.e. the Ag plate and AgI and Ag_2S pellets, all of which exhibit some ductility, were broughtinto a closercontact by mechanical assistance.

The circuit model in Fig. 1(a) can be constructed using the Jamnik-Maier model (DX-15) and the geometric capacitor C_{dielec} in series. For the fitting, an inductor was connected additionally in series (not shown). The fitted results shown in Fig. 2 and Fig. 3 are essentially the same as previously reported,[7] since the fit model and the nonlinear least squares fitting algorithm using the weighting proportional to the calculated impedance magnitude are exactly the same. Note that the simulated curves in Fig. 2 do not include the inductance and thus display thehigh frequency semi-circular response of *RC* circuit with the bulk resistance $R_{bulk} = (R^{-1}_{ion} + R^{-1}_{eon})^{-1}$ and the geometric capacitance C_{dielec}.

The errors in the individual fit or derived material parameters obtained in the present work and indicated in the plots can, however, shed more light on the reliability of the individual values and thus lead to a more solid analysis. The errors of the directly evaluated fit parameters are indicated in Fig. 3(f). The errors in $C^{\perp}_{eon}$ are shown to indeed diverge with increasing EMF, as suggested in the previous report.[7]

By replacing the chemical capacitors to CPEs with complex capacitance $A(i\omega)^{\alpha-1}$, enabled in the model DX-19 in the Zview program or the Jamnik-Maier-Lai-Lee model, the non-ideal Warburg impedance behavior generally observed in experiments can be described in conjunction with the transmission line model for mixed conductors with variable electrode conditions, as shown in Fig. 1(b). Fig. 4(c) indicates that α values mostly become smaller than the ideal value of 1 except for two points at low EMF. This is typically experimentally observed behavior. Note that a CPE with α larger than 1 leads to a negative value in the real impedance, given by Eq. 10, the physical significance of which is rather doubtful. The spectrum at EMF = 30 mV in Fig. 2 exhibits almost identical fit residuals, since the fitted α value by the DX-19 model is close to 1 for the ideal DX-15 model. It can be seen that the DX-19 model with adjusted α reduces the fit residuals of the low frequency spectra where the main Warburg impedance arc is observed. Figs. 2(d), (e),

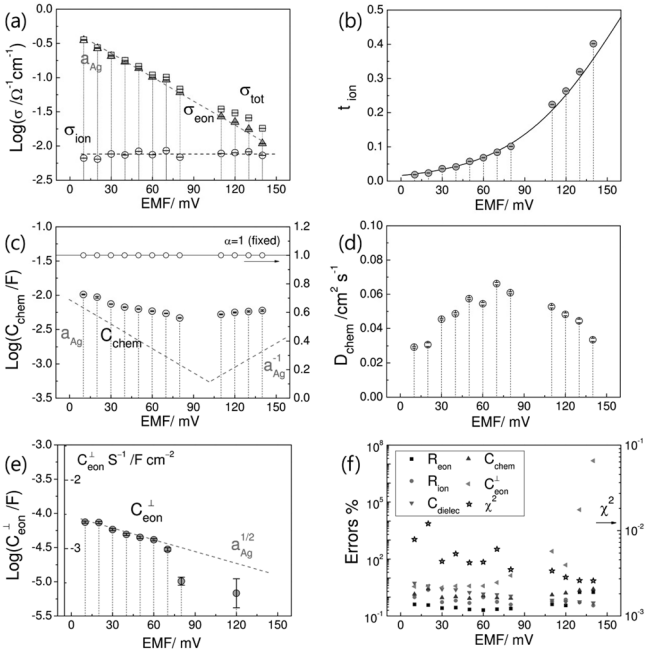

Fig. 3. Fit parameters or material properties therefrom obtained by the ideal transmission line model for mixed conductors with an electron-blocking electrode condition, as indicated in Fig. 1(a).

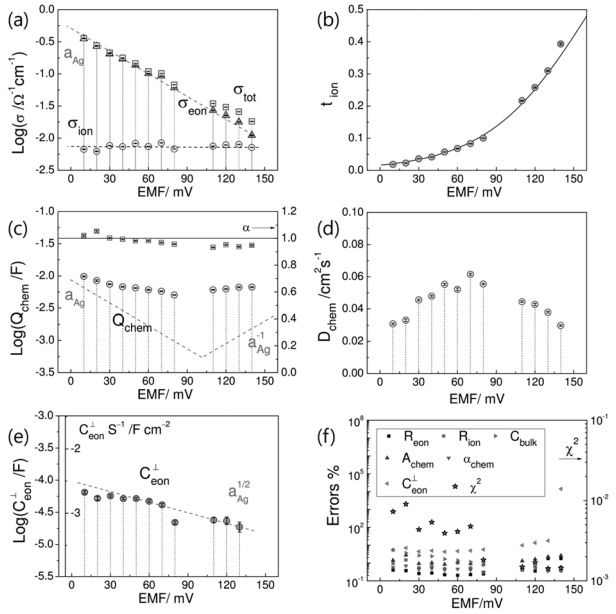

Fig. 4. Fit parameters or material properties therefrom derived in the modified transmission line model where the shunt capacitors for C_{chem} in Fig. 1(a) are replaced by shunt CPEs or Q_{chem} elements, as shown in Fig. 1(b).

and (f) indicate a substantial decrease in the fit residuals by the DX-19 model compared to the DX-15 model at the low frequency range below 10 Hz, which can be ascribed to the variation of α values between 0.93 and 0.97 from the fixed value of 1. This aspect is also clearly represented by the χ^2 values in Fig. 3(f) and Fig. 4(f). The parameter represents the goodness of the fit. For the spectra at 80, 110, 120, 130, and 140 mV, the χ^2 values are shown to decrease to $1.5\sim1.8\times10^{-3}$ from $2.5\sim3.5\times10^{-3}$. It should be noted, however, that the large fit residuals in the spectra at EMF values from 10 mV to 70 mV in the intermediate frequency range remained essentially the same or even became larger in the case of DX-19 compared to DX-15.

Fit parameters represented in Fig. 3 and Fig. 4 do not appear to be significantly different, since the variation of α values was limited between 0.93 and 1.05. The features of the measured and derived parameters can be explained by the well-known defect chemistry of Ag_2S with large ionic disorder, as $c_{ion} \gg c_{eon}$ and c_{ion}~constant, $c_{eon} \propto a_{Ag}$.[11,14,26] The ionic conductivity (σ_{ion}) from $R_{ion} = R_{dc}$ is almost independent of a_{Ag}, consistent with the presence of large ionic disorder in the system (Fig. 3(a) and Fig. 4(a)). The electronic conductivity σ_{eon} from the R_{eon} values increases linearly with a_{Ag} or $\log\sigma_{eon}$ proportional to –EMF, where $EMF = -(RT/F)\ln a_{Ag}$, indicating the electronic concentration follows the classical Boltzmann statistics (Fig. 3(a) and Fig. 4(a)). The ionic transference number (t_{ion}) thus increases from 0.02 to about 0.40 (Fig. 3(b) and Fig. 4(b)). The dependence and the absolute values are consistent with the literature.[27]

The chemical capacitance (C_{chem}, Eq. 7) (Fig. 3(c)) and therefrom derived chemical diffusion coefficient (D_{chem}, Eq. 8) (Fig. 3(d)) exhibit a slight minimum/maximum, respectively. For the generalized transmission line model the effective chemical capacitance Q_{chem} can be estimated according to Eq. 13; the results are not significantly different from C_{chem}, which may be considered consistent with the small non-ideality represented by α values close to the ideal value of 1. Due to the large ionic disorder, C_{chem} in Eq. 7 becomes proportional to the concentration of the electronic species, c_{eon}, which represents both defect electrons and holes. They are proportional to a_{Ag} and a_{Ag}^{1}, respectively. The electronic conductivity indicated in Fig. 3(a) and in Fig. 4(a) can be essentially ascribed to the contribution by the defect electrons, since the electron mobility in Ag_2S is known to be higher than the hole mobility by two orders of magnitude.[27] Therefore, the minimum point in C_{chem} corresponds to the stoichiometric point, as suggested by the dashed lines. (They represent the results from the ion-blocking cell discussed later). However the dependence is far less than expected. The behavior may be explained by the extra chemical storage contribution in the material working independently of the global polarization due to the electrode condition. The grain boundary area in the polycrystalline specimen in the present work can be an additional source for the variation of the silver stoichiometry. The large, correlated real and imaginary fit residuals of the transmission line models, DX15 and DX19, compared to the KK residuals in the spectra in Figs. 2(a) to (d), may be considered to indicate the model inadequacy in describing the additional contribution.

The stoichiometric point suggested by the minimum appears to be somewhat lower than values reported in the literature, which range between 120 mV and 150 mV.[11,27] The maximum point in the chemical diffusivity D_{chem} shifts to a further lower value due to the resistance factor when estimated according to Eq. 8. Since the values are derived from C_{chem}, the results are characterized by a much less pronounced peak than previously reported.[26]

The fit parameter most affected by the generalization appears to be $C_{eon}^{\perp}$ in Fig. 4(e), as compared to Fig. 3(e). The guide line indicates the theoretical dependence according to Eq. 9. $C_{eon}^{\perp}$ is proportional to $\sqrt{c_{eon}}$ and thus to $a_{Ag}^{1/2}$. Note that the missing data points compared with other parameters are below the lower boundary of the graph and are associated with large errors, as indicated in Fig. 3(f) and Fig. 4(f). In contrast to the analysis by the ideal Jamnik-Maier model (DX-15), $C_{eon}^{\perp}$ can be estimated for an EMF range between 80 and 130 mV with reasonable error (max. 17%), and the results follow the dependence of $a_{Ag}^{1/2}$, as clearly indicated by the lower EMF data by the DX-15 model in Fig. 3(e). It is also noted that the $C_{eon}^{\perp}$ estimation for EMF 10 mV and 20 mV became poorer in view of the increased errors and the deviation from $a_{Ag}^{1/2}$ dependency. The feature appears to be correlated with the Q element, with a values 1.021 and 1.054 larger than the ideal value, which results in negative real impedance. Although $C_{eon}^{\perp}$ values with consistent EMF dependence can be reliably obtained over a wider EMF range by employing the generalized transmission line model, the values remain far too large, as discussed previously. The value is ca. 10^4 times the value estimated using the electron concentrations of Ag_2S.[9] The behavior cannot be explained by the additional large capacitance values indicated in the chemical capacitance. The capacitance is likely dominated by the charge adsorption at the core of the interface, which also appears to be proportional to $a_{Ag}^{1/2}$.

It is generally true that an increased number of components or variables in the model results in a better description of the overall spectra, which is also represented by decreased fit residuals as representedin the bottom graphs of Fig. 2. This is also the principle of the numerical Kramers-Kronig test, namely, employing many resistor-capacitor or other KK-compliant components to simulate the spectra as well as possible[28] and thus to show the KK validation of the measured impedance spectra. With regard to the parameter estimation, however, the components with slightly different relaxation times are subject to large statistical errors and the physical significance of the parameters becomes less clear. A similar situation may occur with the generalization of the ideal capacitor elements to the CPEs of the complex capacitance $A(i\omega)^{\alpha-1}$, which is allowed in the DX-19 modelor the 'Jamnik-Maier-Lai-Lee' model. It should

be also noted that CPEs with $\alpha < 1$ extend over a much wider frequency range than combinations of the ideal R and C elements. Therefore, the CPEs often powerfully describe the overall complicated spectral feature, as also will be demonstrated in the next section of the present work.

In an attempt to reduce the large fit residuals shown in Fig. 2 an analysis has been carried out with the interfacial capacitance $C_{\mathrm{eon}}^{\perp}$ generalized to Q elements. It does not, however, substantially improve the goodness of the fit, thus indicating a different origin of the model discrepancy. In fact, with a slight improvement in the fitting quality, the fitted parameters with the generalized $C_{\mathrm{eon}}^{\perp}$ become less reliable. In general, the CPE can apparently describe the experimental spectra quite satisfactorily and often the parameters A and α are found to be associated with small errors. The two parameters, A and α, of the CPE are, however, often correlated with each other and also correlated with other parameters in the model. The physicochemical properties represented by the material parameters can be obscured and the material parameters may become less accurate, unless CPEs exhibit characteristic values from the underlying mechanism. The analysis with the generalized $C_{\mathrm{eon}}^{\perp}$ as well as C_{chem} increases the errors of the fit parameters, and a slight systematic tendency, as indicated in Fig. 3 and Fig. 4, is observed. The deteriorated quality in the $C_{\mathrm{eon}}^{\perp}$ for EMF 10 and 20 mV associated with α values larger than 1 for the generalized chemical capacitance may also be considered as an excessive generalization.

4.2. Pt|Ag$_2$S|Pt ion-blocking cell

A counterpart configuration can be made using ion-blocking cell of Pt|Ag_2S|Pt, which may be modeled with $R_{\mathrm{ion}}^{\perp} = \infty$ and $R_{\mathrm{eon}}^{\perp} = 0$ in Fig. 1(c). In principle, any metallic electrode different from the components of the mixed conductors can be used as ion-blocking electrodes. Platinum has been used for silver chalcogenides in earlier experiments.[10,13] Unlike the ion-blocking electrode AgI, which can be practically used only above 147°C at the high temperature superionic phase, the electron-blocking electrodes are not limited in application temperature, as demonstrated by Hebb.[10] Yokota[13] reported the polarization/depolarization response for a Pt|Ag_2Te|Pt cell, which can be equivalently represented in the frequency domain response. Ion-blocking electrodes mostly have been applied for electronic conductivity measurements in oxide ion electrolytes by the dc method.[29,30] Lai et al[6] demonstrated the application of the Jamnik-Maier model on ceria with mixed oxygen and electron conduction with Pt electrodes. However, no impedance spectroscopy for the classical Pt|Ag_2X|Pt cell for the mixed conducting silver chalcogenides Ag_2X has been reportedyet. Therefore, the results displayed in Fig. 5 may be the first report of its kind.

From the mixed conduction characteristics shown above in the electron-blocking electrode condition, a large variation of the dc limit corresponding to the variation in R_{eon} with silver activity is expected, which is also qualitatively illustrated in Fig. 5. However, the absolute conductivity values and the silver activity dependence appear not to be in good agreement. In fact, the description or modelling of the complicated spectral feature, as indicated in the insets of Fig. 5, appears to be a formidable task if not impossible. Even the full generalization of $C_{\mathrm{ion}}^{\perp}$ as well as C_{chem} to Q elements resulted in a far too unsatisfactory description. A strongly non-ideal Warburg-like impedance character is indicated for some of the highest EMF cases, as shown in Figs. 5(e) and (f) for EMF 120 mV and 140 mV, respectively, but the low frequency limits tend to curl inside, leading to a substantially smaller dc limit value. The behavior is in contrast to the behavior of the electron-blocking cell, where the cell tends to become disconnected and thus strongly resistive unless the interfaces are brought into stable mechanical contact. In spite of the highly non-trivial spectral feature, the Kramers-Kronig residuals in the bottom graphs indicate the validity of the impedance data for the model analysis. (As in the electron-blocking cell, the quality of the spectra around 1 MHz are adversely affected by instrumental artefacts).

Some characteristic spectral features can be noted for the model development. First, the Warburg impedance at the low frequency range, although the magnitude of the impedance is small and hardly distinguishable for low EMF values, is far from the ideal behavior; generalization of C_{chem} to Q_{chem} by the DX-19 model hence appears essential. The low frequency curling behavior cannot be described by the present model and thus the concerned low frequency data should not be included for the analysis. Second, an additional impedance contribution appears to be located in the intermediate frequency range between high frequency bulk and low frequency Warburg impedance, as indicated in Figs. 5(c) to (f). The contribution may be considered as a charge transfer impedance, which may be modeled by a separate RC or RQ parallel circuit.[15-17,25] It should be noted that $R_{\mathrm{eon}}^{\perp}$ is not the charge transfer resistance at the interface but may represent the degree of blocking. Charge transfer impedance may be modeled as an extra component for the ideally blocking $R_{\mathrm{ion}}^{\perp} = \infty$ and ideally permissive $R_{\mathrm{eon}}^{\perp} = 0$ electrode condition. Third, the dc limit, especially for the high EMF data, is substantially smaller than the expected by the electronic conductivity, even without consideration of the curling behavior. The curling phenomena may be attributed to incomplete blocking of the Pt electrodes, as Ag can locally accumulate and possibly create a solid solution with Pt to some extent. However, the incomplete blocking should notaffect the high frequency bulk impedance. From the spectra in Figs. 5(e) and (f), where the bulk response and the Warburg response are distinguished, it can be shown that the bulk response is reduced in similar proportion. The behavior may be modeled by a conduction path in parallel to the sample response. If the sample response is constituted by two individual resistors in series with the respective capacitive effects, the original resistor components could not be deconvoluted when short-circuiting occurs. However,

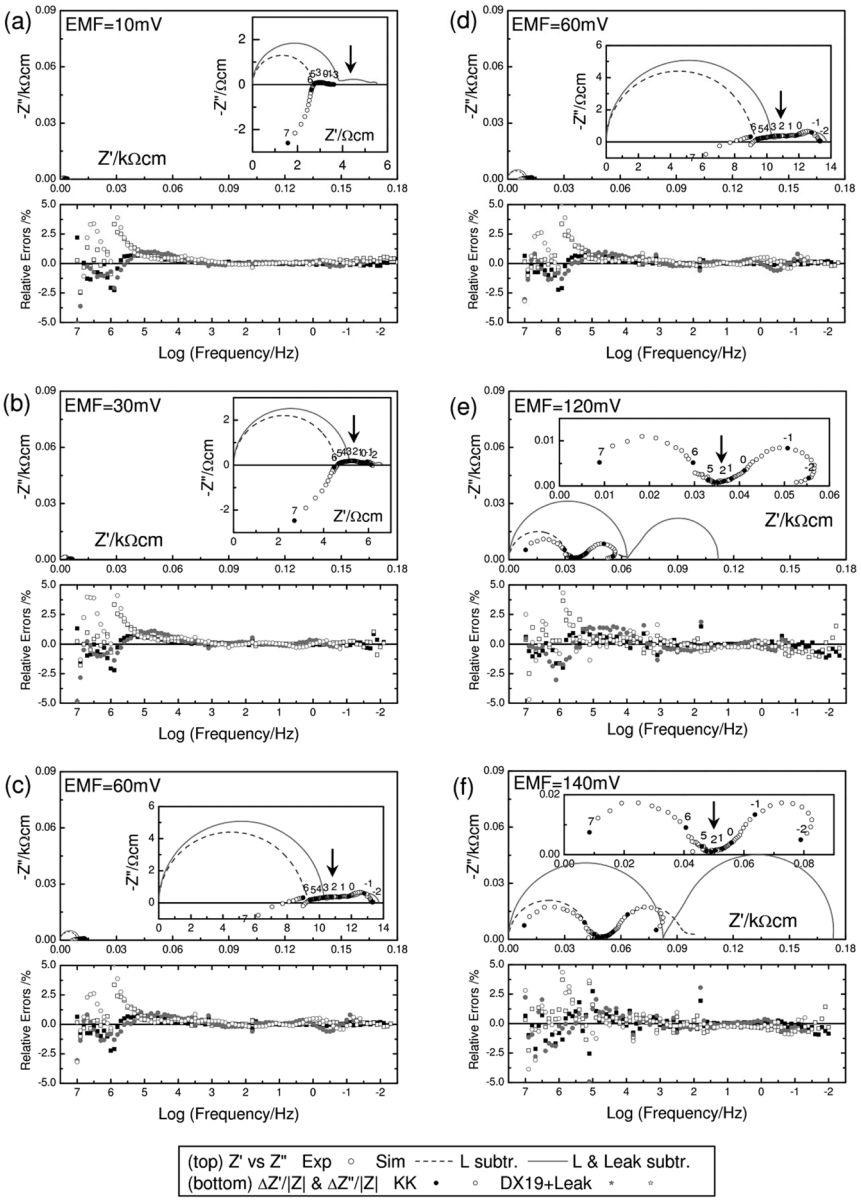

Fig. 5. Impedance spectra of $Pt|Ag_2S|Pt$ with EMF of the galvanic cell of 10, 30, 60, 90, 120, and 140 mV. The lines indicate the simulation according to the fit results using the generalized equivalent circuit in Fig. 1 (DX15) and with chemical capacitors replaced by Q_{chem} (DX19) and additional Q_{leak} with α close to zero. The simulated curves with the Q_{leak} subtracted indicate the spectral feature originally expected from the cell construction. In the simulated curves the inductor elements were subtracted.

according to the transmission line model, the high frequency and low frequency components are related as $R_{bulk} = (1/R_{ion} + 1/R_{eon})^{-1}$ and $R_{dc} - R_{bulk} = R_{eon} - (1/R_{ion} + 1/R_{eon})^{-1}$ and the shunt capacitance cannot be attributed to the lower frequency impedance component only.

Indeed, modelling of the parallel resistor to the transmission line model turned out to be a breakthrough and the experimental spectra could indeed be reasonably described. The nature of the short-circuiting path within the sample should be clarified. It may comprise grain boundaries in the polycrystalline Ag_2S sample, which may have different defect concentration and non-stoichiometry. On the other hand, appreciable short-circuiting boundary effects are not seen in the more ideally behaving spectra under the electron-blocking condition in Fig. 2. It is also suggested in the previous section that such inhomogeneous areas or regions, if not active as overall short-circuiting paths, may be responsible for the extra chemical capacitance effects observed in the electron-blocking condition shown in Fig. 3(c) or Fig. 4(c). It is conceivable that internal boundaries connected in three dimensions, as in a brick-layer model, can be conductive or capacitive depending on the transport species and terminal condition.[31]

It is thus also physically plausible to model the short-circuiting path as a CPE, indicated as Q_{leak} in Fig. 1(c), rather than as a pure resistor element. With α of zero, the Q ele-

ment with admittance $A\,(i\omega)^{\alpha}$ is a resistor element. The fit result of Q_{leak} shown in Fig. 6(g) indicates leak resistance or conductance proportional to that of the sample. α values are close to zero, but can be as large as 0.2. Additional generalization of $C_{\mathrm{ion}}^{\perp}$ to the Q element or modelling extra charge transfer impedance was found to be excessive. The impedance contribution in the middle frequency range, indicated by arrows in Fig. 5, is shown to be successfully described by a non-zero $R_{\mathrm{eon}}^{\perp}$ of ca. $10\,\Omega$ or $0.25\,\Omega\,\mathrm{cm}^2$, as shown in Fig. 6(f). The contribution in the impedance spectra in Fig. 5 is twice the value due to the symmetric electrode condition, Fig. 1(c) and normalized with respect to the sample geometry, corresponding to $2 \times 0.17\,\Omega$ cm. The values can be identified in the insets of the calculated spectra in Fig. 5(a), (b), (c) and (d) for low EMF values. It should be noted, however, thatthis value in the the measured impedance spectrais further reduced due to the short-circuiting and thus correspondingly changed.

The triumph of this modelling approach is shown in the parameter estimation in Figs. 6(a), (b), (c), (d), and (e). Partial conductivities, chemical capacitance, chemical diffusivity, and interfacial capacitance ascribed to the ionic charge carriers are consistent with the material properties, although associated with rather large errors. The partial conductivities shown in Fig. 6(a) are relatively consistent with those obtained from the electron-blocking cell in Fig. 3(a) or Fig. 4(a). This is clearly shown by the simulated curves in Fig. 5 with Q_{leak} subtracted. Substantial deviation (as much as 0.7) of α of the chemical capacitance or Q_{chem} is indicated for the low EMF case in Fig. 6(c). The effective chemical capacitance value now clearly indicates the theoretical a_{Ag} and a_{Ag}^{-1} dependence with a well-defined minimum around 90~110 mV. The chemical diffusivity D_{chem} derived therefrom thus exhibits a sharper maximum close to the peaked behavior reported in the literature.[26] The large and constant $C_{\mathrm{ion}}^{\perp}$ is also consistent with the large ionic disorder in the material.

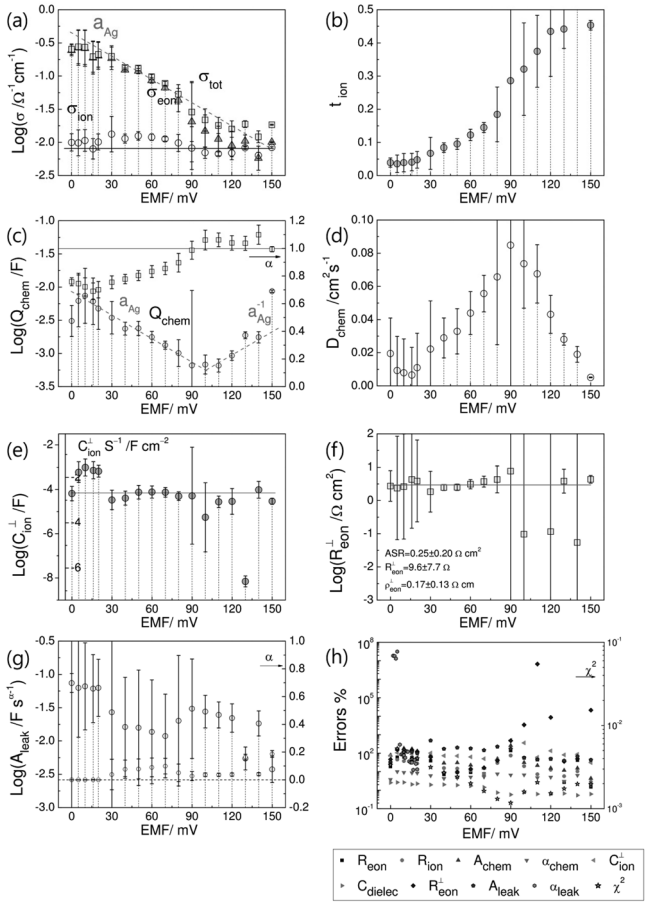

Fig. 6. Fit parameters or therefrom derived material parameters in the modified transmission line model with electron-blocking or ion blocking electrodes shown in Fig. 1(c). The leakage was modelled by Q element (Q_{leak}), which behaves close to the ideal resistor.

5 Conclusion

The generalized equivalent circuit model for mixed conductors with semi-blocking electrodes suggested by Jamnik and Maier can be expanded for the practical analysis of the so-called 'generalized Warburg impedance' by replacing the ideal capacitor elements in the *RC* transmission line model with constant phase elements (CPEs) having complex capacitance $A(i\omega)^{\alpha-1}$. The expansion has been recently implemented as the Jamnik-Maier-Lai-Lee Model (DX19) in the commercial program Zview and applied to a model mixed conductor Ag_2S both in an electronically and ion-blocking configuration, i.e., Ag | AgI | Ag_2S | AgI | Ag and Pt | Ag_2S | Pt. The electrochemical cell with electron-blocking AgI electrodes exhibited almost an ideal Warburg feature with correct partial conductivity values and a slight differenceresultedfrom the generalization of the shunt capacitors for the chemical capacitance by CPEs. The chemical capacitance values were, however, too large and did not show the expected silver activity dependence. On the other hand, the impedance response of the ion-blocking Pt | Ag_2S | Pt cell, the first report ofits kind, turned out to be extremely non-trivial. Modelling a leakage circuit to the generalized transmission line model with shunt CPEs was found to provide an adequate description of the spectral features and a consistent set of material parameters was also successfully deconvoluted. It is suggested that the internal boundaries with extra chemical storage in Ag_2S may be the origin of the unusually high chemical capacitance in the electron-blocking configuration and the presence of the short-circuiting path in the ion-blocking configuration.

Acknowledgment

This work was supported by a National Research Foundation of Korea (NRF) grant funded by the Korean government(MEST)(KRF-2008-531-D00006). The authors thank Derek Johnson at Scribner Associates for implementing the generalized transmission line model (DX19) in the software package ZView to enable the analysis presented here.

REFERENCES

1. E. Yi, M. Yoon, J. Moon, and H. Hwang, "Fabrication of a$MnCo_2O_4$/gadolinia-doped Ceria (GDC) Dual-phase Composite Membrane for Oxygen Separation," *J. Kor. Ceram. Soc.,* **47** [2] 199-204 (2010).
2. J.-Y. Park, J.-S. Park, Y.-T. Kim, and K.-H. Hur, "Thermally Stimulated Depolarization Current Test for Reliability of X5R MLCC," *J. Kor. Ceram. Soc.,* **46** [2] 155-60 (2009).
3. J. Jamnik and J. Maier, "Treatment of the Impedance of Mixed Conductors Equivalent Circuit Model and Explicit Approximate Solutions," *J. Electrochem. Soc.*, **146** [11] 4183-88 (1999).
4. J. Jamnik, J. Maier, and S. Pejovnik, "A Powerful Electrical Network Model for the Impedance of Mixed Conductors," *Electrochimica Acta,* **44** 4139-145 (1999).
5. J. Jamnik and J. Maier, "Generalised Equivalent Circuits for Mass and Charge Transport: Chemical Capacitance and its Implications," *Phys. Chem. Chem. Phys.*, **3** 1668-678 (2001).
6. W. Lai and S. M. Haile, "Impedance Spectroscopy as a Tool for Chemical and Electrochemical Analysis of Mixed Conductors: A Case Study of Ceria," *J. Am. Ceram. Soc.,* **88** 2979-997 (2005).
7. J.-S. Lee, J. Jamnik, and J. Maier, "Generalized Equivalent Circuits for Mixed Conductors: Silver Sulfide as a Model System," *Monatsh. Chem.,* **140** [9] 1113-119 (2009).
8. C. Wagner, "Üeber Die Natur Des Elektrischen Leitvermogens Des α-Silbersulfids," *Z. Phys. Chem.,* **21** 42-7 (1933).
9. S. Miyatani, "On the Polarization of Silver Sulfide," *J. Phys. Soc. Jpn.,* **10** 786-93 (1955).
10. M. H. Hebb, "Electrical Conductivity of Silver Sulfide," *J. Chem. Phys.,* **20** 185-90 (1952).
11. C. Wagner, "Investigation on Silver Sulfide," *J. Chem. Phys.,* **21** [10] 1819-827 (1953).
12. C. Wagner, "Equations for Transport in Solid Oxides and Sulfides of Transition Metals," *Prog. Solid State Chem.,* **10** 3-16 (1975).
13. I. Yokota, "On the Theory of Mixed Conduction with Special Reference to Conduction in Silver Sulfide Group Semiconductors," *J. Phys. Soc. Jpn.,* **16** 2213-223 (1961).
14. H. Schmalzried, "Ag_2S-the Physical Chemistry of an Inorganic Material," *Prog. Solid State. Chem.,* **13** 119-57 (1980).
15. J. Maier, "Evaluation of Electrochemical Methods in Solid State Research and Their Generalization for Defects with Variable Charges," *Z. Phys. Chem. N.F.,* **140** 191-215 (1984).
16. J.-S. Lee and H.-I. Yoo, "Direct Measurement of Partial Ionic Conductivity of $Co_{1-\delta}O$ Via Impedance Spectroscopy Combined with DC Relaxation," *Solid State Ionics,* **68** 139-49 (1994).
17. J.-S. Lee and H.-I. Yoo, "A New Assessment of Ionic Conductivity of YBa_2Cu_3Ox Via AC Impedance Spectroscopy Combined with DC Relaxation," *J. Electrochem. Soc.,* **142** [4] 1169-176 (1995).
18. D. Johnson, "ZView: A Software Program for IES Analysis, Version 3.2 c," 2010.
19. K. Cole and R. Cole, "Dispersion and Absorption in Dielectrics I. Alternating Current Characteristics," *J. Chem. Phys.,* **9** 341-51 (1941).
20. B. Boukamp, Equivalent Circuit (Equivcrt.PAS) Users Manual, Report CT89/2 14/128, The Netherlands, University of Twente, 1989.
21. J. Fleig, H.-R. Kim, J. Jamnik, and J.Maier, "Oxygen Reduction Kinetics of Lanthanum Manganite (LSM) Model Cathodes: Partial Pressure Dependence and Rate-Limiting Steps," *Fuel Cells,* **8** [5] 330-37 (2008).
22. J. Jamnik, "Impedance Spectroscopy of Mixed Conductors with Semi-Blocking Boundaries," *Solid State Ionics,* **157** 19-28 (2003).
23. E.-C. Shin, S. M. Seo, H.-H. Park, S. J. Kim, C. H. Kim, D. J. Kim, C. K. Hong, G. Seo, and J.-S. Lee, "Transmission Line Model for the Percolating Carbon Network in the Dielectric Matrix: Part I. Theory," *Phys. Chem. Chem. Phys.*, submitted.
24. S. M. Park, H.-H. Seo, E.-C. Shin, S. J. Kim, C. H. Kim, D. J. Kim, C. K. Hong, G. Seo, and J.-S. Lee, "Transmission Line Model for the Percolating Carbon Network in the Dielectric Matrix: Part I. Applications to Rubber Composits," *Phys. Chem. Chem. Phys.*, submitted.
25. R. Andreaus and W. Sitte, "Ionic Transport Properties of Mixed Conductors: Application of AC and DC Methods to Silver Telluride," *J. Electrochem. Soc.*, **144** [3] 1040-44 (1997).
26. K. D. Becker, H. Schmalzried, and V. von Wurmb, "The Chemical Diffusion Coefficient in (Low Temperature) α-Ag_2S Determined by an Electrochemical Relaxation Method," *Solid State Ionics*, **11** [3] 213-19 (1983).
27. G. Bonnecaze, A. Lichanot, and S. Gromb, "Proprietes Electroniques Et. Electrogalvaniques Du Sulfure D'Argent α : Domaine D'Existence," *J. Phys. Chem. Solids,* **39** 299-310 (1978).
28. B. A. Boukamp, "Practical Application of the Kramers-Kronig Transformation on Impedance Measurements in Solid State Electrochemistry," *Solid State Ionics,* **62** 131-41 (1993).
29. L. Burke, H. Rickert, and R. Steiner, "Elektrochemische Untersuchungen zur Teilleitfähigkeit, Beweglichkeit und Konzentration der Elektronen und Defektelektronen in dotiertem Zirkondioxid und Thoriumdioxid," *Z. Phys. Chem.,* **74** [3-6] 146-67 (1971).
30. W. Zipprich and H. Wiemhöfer, "Measurement of Ionic Conductivity in Mixed Conducting Compounds using Solid Electrolyte Microcontacts," *Solid State Ionics,* **135** [1] 699-707 (2000).
31. J. Maier, "Nanoionics: Ion Transport and Electrochemical Storage in Confined Systems," *Nature Mater.,* **4** [11] 805-15 (2005).